New Methods for Computation of the Inductance Matrix of Transformer Windings for Very Fast Transients Studies

M. Eslamian and B. Vahidi, *Senior Member, IEEE*

Abstract—To study very fast transients in transformers, computing the winding inductance matrix at very high frequencies (MHz) is required. The air-core approximation formulas cannot be used for this purpose because at very high frequencies the core behaves as a magnetic insulating wall and so the distribution of the magnetic field is quite different from that of air-core inductors. This paper presents new analytical methods for computing the winding inductance matrix at very high frequencies considering the presence of the core. A simple method, based on numerical integration of the vector potential functions, is described for the calculation of inductance outside the core window. For the region inside the core window, two different analytical solutions are developed and inductance formulas are extracted. The final expressions are simple and fast convergent. Comparisons with finite-element method simulations prove the high accuracy of the technique.

Index Terms—Inductance matrix, magnetic fields, transformer winding, very fast transients.

I. INTRODUCTION

THE DETAILED model of winding consisting of inductive, capacitive, and loss components has been used widely for the analysis of fast and very fast transients in transformers [1]–[15]. For very fast transients, such as those caused by switching operations in gas-insulated substations (GIS), using one segment per turn in order to achieve the required detail of the winding model [16] is needed. In very fast front transients, the flux penetration into core is negligible. The core acts as a flux barrier at very high frequencies and the distribution of the magnetic field is quite different from that of air-core inductors. This is more significant in the core window. At high frequencies, the core window shapes the distribution of the magnetic flux, affecting the values of self and mutual inductances. Very large errors have been reported when the self and mutual inductances are computed with the commonly used air-core approximations [17]. The consequence of this is that the transient response of a winding is not properly computed when the core is represented as air.

The FEM analysis is an accurate method for the calculation of inductance which is able to consider the details of the transformer geometry [18]. However, this method is computationally expensive. Computation of winding impedances at high frequencies is described in [19]. It offers theoretically accurate results but its implementation is rather complicated. Recently, a technique, based on the application of a multilayer method of images, was presented in [17] to take the presence of the core into consideration. The mutual flux between round conductors is computed by successively adding layers of images one at a time and computing the relative difference between consecutive values. The procedure stops when the difference is lower than a fixed quantity.

In this paper, new analytical methods for computing the inductance matrix of transformer windings with conductors of the rectangular cross section at high frequencies are presented. Two distinct regions are considered for the inductance calculation: 1) outside the core window and 2) inside the core window. The total inductance is obtained by means of a weighted addition of the components from each region depending on the specific transformer geometry [17].

For the region outside the core window, the core wall is replaced by an image source with the correct magnitude and location and then by integrating the vector potential produced by actual and image sources over the cross section of the target coil (or conductor), the self and mutual inductances are calculated.

For computation of inductance inside the core window, two different methods are developed in this paper. Both methods are based on an analytical solution of the Poisson equation in planar coordinates. The boundary conditions are flux parallel for all edges of the core window. In the first method, a double Fourier series is applied to the current density and then using the method of the separating variables, a solution in the form of a double series of harmonics is obtained for the vector potential. The method of double Fourier series has been used before for calculation of the leakage reactance of transformer windings [20]. The method developed in this paper utilizes the same procedure but it uses different boundary conditions to represent the core behavior at very high frequencies.

In the second method, the solution space is divided into three regions and a single Fourier series in terms of a fundamental period of the window height is applied to the current density. Using the separating variables and then applying the required constraints to the solutions for satisfying the boundary conditions, the vector potential in each region is obtained as a single series of sine and exponential components. This method is also
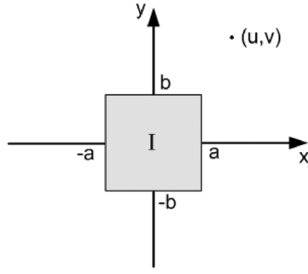
Fig. 1. Coil of a rectangular cross section in the air.

Fig. 2. Coil of the rectangular cross section in air.

an extension of the Rabins' method [21], [22] in planar coordinates and with different boundary conditions.

In both methods presented in this paper, the inductances are calculated by applying the magnetic energy method. Simulation results show that both methods produce the same results up to at least six digits. Although the inductance formula obtained by the double Fourier series method is rather simpler, it takes more time to evaluate than the inductance formulas obtained by the single Fourier series method. One advantage of the single Fourier series method is that it can be developed easily in order to extract inductance expressions in axisymmetric coordinates. Despite these differences, both techniques are fast convergent and can be used to compute the inductance matrix inside the core window with high accuracy. The results of the proposed formulas for the self and mutual inductances are verified with finite-element analyses and the relative differences are compared with those of the previously presented multilayer image method [17].

II. OUTSIDE THE CORE WINDOW

A. Calculation of Vector Potential

The vector potential produced by a coil having a uniform current density can be found by integrating the vector potentials of an infinite number of line currents which can be deemed to constitute the distributed current. The starting point is the expansion of the vector potential of a line current

$$A = -\frac{\mu_0 I}{2\pi} \ln(r) + A_0 \qquad (1)$$

where r is the distance from the source to the point at which A exists and A_0 is a constant term. For a single line current, A_0 approaches infinity but for a multiconductor system with zero net current, A_0 can be dropped from the equation and only the first term can be used to calculate the vector potential component produced by each conductor.

Fig. 1 shows a coil of rectangular cross section with sides of length 2a and 2b in the air. For a current I in the coil, the current density is $I/4ab$.

The current carried by a filament of cross section $dx'dy'$, where x' and y' are coordinates of any filament in the coil, is $(I/4ab)dx'dy'$. The vector potential produced by all elements of the coil is given by substituting for I in (1) and integrating over the cross section of the rectangle (with $A_0 = 0$). The vector
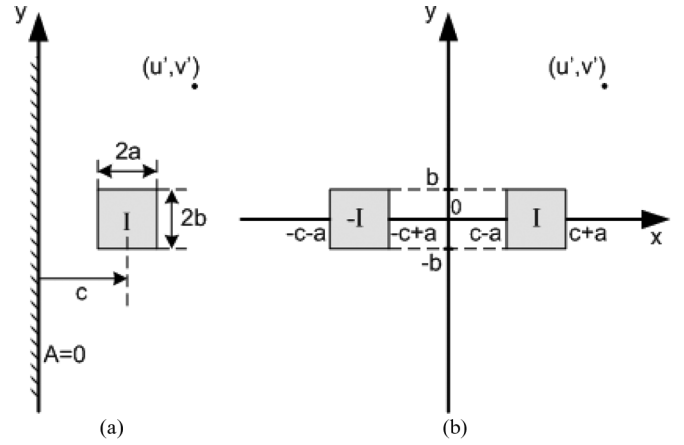
potential at any point (u,v) can be integrated in terms of simple functions. The result is

$$
\begin{aligned}
A = -\frac{\mu_0 I}{16\pi ab} \Bigg(& (b-v)(a-u)\ln\left((b-v)^2+(a-u)^2\right) \\
& + (b-v)(a+u)\ln\left((b-v)^2+(a+u)^2\right) \\
& + (b+v)(a-u)\ln\left((b+v)^2+(a-u)^2\right) \\
& + (b+v)(a+u)\ln\left((b+v)^2+(a+u)^2\right) \\
& + (b-v)^2\left(a\tan\left((a-u)/(b-v)\right)\right. \\
& \qquad\qquad \left. +a\tan\left((a+u)/(b-v)\right)\right) \\
& + (b+v)^2\left(a\tan\left((a-u)/(b+v)\right)\right. \\
& \qquad\qquad \left. +a\tan\left((a+u)/(b+v)\right)\right) \\
& + (a-u)^2\left(a\tan\left((b-v)/(a-u)\right)\right. \\
& \qquad\qquad \left. +a\tan\left((b+v)/(a-u)\right)\right) \\
& + (a+u)^2\left(a\tan\left((b-v)/(a+u)\right)\right. \\
& \qquad\qquad \left. +a\tan((b+v)/(a+u))\right) - 12ab\Bigg).
\end{aligned}
$$

$$(2)$$

The vector potential of additional coils is given by superposition of their particular vector potentials.

Fig. 2(a) shows a coil of rectangular cross-section outside the core window. At high frequencies, the core leg can be represented by an infinite vertical line corresponding to a magnetic insulation boundary. This type of boundary can be replaced by an image coil carrying the same current as the real one but in the opposite direction [see Fig. 2(b)].

To obtain the vector potential at any point outside the window, one needs to account for the effects of the image and actual coils simultaneously. By superposition of the vector potentials produced by both coils, A at any point $(u', v')(u', v' > 0)$ is obtained as

$$A = A_+ + A_- \qquad (3)$$

where A_+ is the vector potential produced by the actual coil and A_- is the one produced by the image coil.

The values of A_+ and A_- can be calculated using (2). The only thing needed is that for the calculation of A_+, $(u' - c, v')$, and for the calculation of A_-, $(u' + c, v')$ must be substituted for (u,v) in (2). This is necessary because in derivation of (2), it is assumed that the origin of the coordinate system coincides with the center of the coil and, therefore, coordinate shifting is needed in conditions where the coordinates of the viewpoint are measured against points other than the coil's center.

B. Inductance Calculation

Once the vector potential is calculated, it is possible to calculate self and mutual inductances. Consider two coils outside the core window. The mutual inductance between coil 1 and coil 2 with uniform current densities J_1 and J_2 is given by

$$M_{12} = \frac{1}{I_1 I_2} \int_{V_1} J_1 . A_2 dV_1. \tag{4}$$

By substituting for A_2 from (3), per-unit length, we obtain

$$M_{12} = \frac{1}{I_1 I_2} J_1 \left[\int_{S_1} A_{+,2} ds + \int_{S_1} A_{-,2} ds \right] \quad (H) \tag{5}$$

where S_1 is the cross section of coil 1. Since the vector potential is a smooth function, the integrals of $A_{+,2}$ and $A_{-,2}$ over a rectangular area can be evaluated by the Gauss–Legendre quadrature. It is found that with a quadrature of order 5 (5 points in each coordinate direction of the integration area), sufficient accuracy is obtained. The coordinates of the integration points and their corresponding weights for a "standard" rectangle are given in the Appendix. For an arbitrary rectangle, a transformation is also needed to map the area into the standard rectangle (See the Appendix.)

III. INSIDE THE CORE WINDOW (DOUBLE FOURIER SERIES METHOD)

A. Calculation of Vector Potential

Using Maxwell's equations and choosing the Coulomb gauge, the well-known equation for the vector potential **A** is obtained

$$\nabla^2 \mathbf{A} = -\mu_0 \mathbf{J}. \tag{6}$$

The current density vector **J** is in the z direction and it can be assumed that all the field quantities are independent of z. With these assumptions, (6) in planar coordinates becomes

$$\frac{\partial^2 A_z}{\partial y^2} + \frac{\partial^2 A_z}{\partial x^2} = -\mu_0 J_z. \tag{7}$$

A coil element inside the core window is shown in Fig. 3. The ampere-turn density inside the coil may be considered as being constant and can be written as a function of position

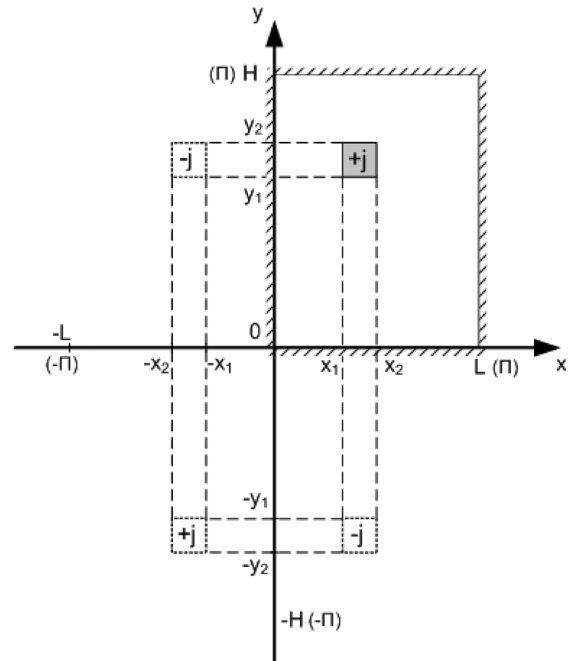$$J(x,y) = \begin{cases} j & x_1 < x < x_2, y_1 < y < y_2 \\ 0 & \text{else} \end{cases} \tag{8}$$

Fig. 3. Reflections of the source relative to the left and bottom wall.

where

$$j = \frac{NI}{(x_2 - x_1)(y_2 - y_1)}. \tag{9}$$

and NI is the ampere-turns of the coil.

A double Fourier series can be applied to the current density. With a doubly harmonic series, we mean a series with terms like cos(mx)cos(ny). Depending on the extension of the current density function, different kinds of product terms appear in the series. To find the correct form, one needs to consider the boundary conditions at the window walls. Fig. 3 also shows images of the coil relative to the left and bottom walls of the window which satisfy the flux parallel boundary condition $(A = 0)$ at these walls. Considering the images from the other sides and those reflected from mirrors on the opposite sides, one may notice that the system of real and image coils repeats at intervals of 2π along the vertical and horizontal axes while the window width and the window height are π radians in terms of the fundamental of the wave.

Considering the sign of the reflections, the following double Fourier series can be used for the current density:

$$J_z = \sum_{m=1}^{\infty} \sum_{n=1}^{\infty} J_{mn} \sin\left(\frac{m\pi}{L}x\right) \sin\left(\frac{n\pi}{H}y\right) \tag{10}$$

where the mnth harmonic coefficient (J_{mn}) is obtained by the equation

$$J_{mn} = \frac{4j}{mn\pi^2} \left(\cos\left(\frac{m\pi}{L}x_1\right) - \cos\left(\frac{m\pi}{L}x_2\right) \right) \\ \left(\cos\left(\frac{n\pi}{H}y_1\right) - \cos\left(\frac{n\pi}{H}y_2\right) \right). \tag{11}$$
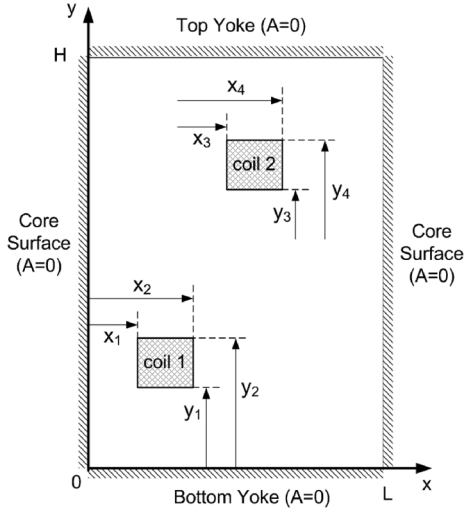
Fig. 4. Two coils inside the core window.

Fig. 5. Solution regions inside the core window.

Substituting the double Fourier series (10) into (7) and dropping the z subscript, we have

$$\frac{\partial^2 A}{\partial y^2} + \frac{\partial^2 A}{\partial x^2} = -\mu_0 \sum_{m=1}^{\infty} \sum_{n=1}^{\infty} J_{mn} \sin\left(\frac{m\pi}{L}x\right) \sin\left(\frac{n\pi}{H}y\right). \tag{12}$$

From (12), A is obtained as

$$A = \sum_{m=1}^{\infty} \sum_{n=1}^{\infty} A_{mn} \sin\left(\frac{m\pi}{L}x\right) \sin\left(\frac{n\pi}{H}y\right) \tag{13}$$

where

$$A_{mn} = \frac{\mu_0 J_{mn}}{\left(\frac{m\pi}{L}\right)^2 + \left(\frac{n\pi}{H}\right)^2}. \tag{14}$$

B. Inductance Calculation

Consider two coils inside the core window as shown in Fig. 4. By substituting for A_2 (the solution of vector potential for coil 2) and J_1 (the double Fourier series of the current density for coil 1) in (4), after some algebraic manipulation, we obtain

$$M_{12} = \frac{LH}{4I_1 I_2} \sum_{m=1}^{\infty} \sum_{n=1}^{\infty} J_{mn,1} A_{mn,2} \quad (H) \tag{15}$$

where M_{12} is the mutual inductance (per unit length) of two arbitrary coils inside the core window.

IV. INSIDE THE CORE WINDOW (SINGLE FOURIER SERIES METHOD)

A. Calculation of Vector Potential

As is shown in Fig. 5, the solution space is divided into three regions. Radial and axial extensions of all regions are given in Table I. The current density can be written as a Fourier series in terms of the yoke-to-yoke distance or window height. For this purpose, as illustrated in Fig. 6, the current density is extended

TABLE I
RADIAL AND AXIAL EXTENSIONS OF REGIONS

Region I	$0 \leq x \leq x_1$	$0 \leq y \leq H$
Region II	$x_1 \leq x \leq x_2$	$0 \leq y \leq H$
Region III	$x_2 \leq x \leq L$	$0 \leq y \leq H$

Fig. 6. Reflection of the source relative to the bottom wall.

as an odd function of period 2H and then a Fourier sine series is applied

$$J_z = \sum_{n=1}^{\infty} J_n \sin\left(\frac{n\pi y}{H}\right). \tag{16}$$

TABLE II
SOLUTION OF A INSIDE THE REGIONS

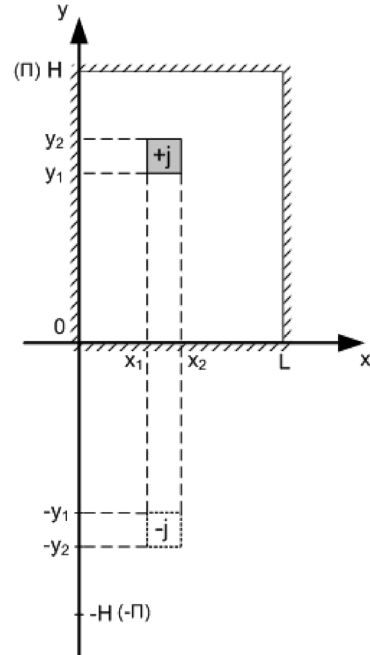| Region I	$A^I = \mu_0 \sum_{n=1}^{\infty} \frac{J_n}{m^2} B_n \left(e^{mx} - e^{-mx}\right) \sin(my)$	$B_n = C_n + \frac{1}{2} e^{-mx_1}$
Region II	$A^{II} = \mu_0 \sum_{n=1}^{\infty} \frac{J_n}{m^2} \left(C_n e^{mx} + D_n e^{-mx} + 1\right) \sin(my)$	$C_n = \frac{e^{-mh}}{1-e^{-2mh}} \left(e^{-mh} \cosh(mx_1) - \cosh(m(x_2-h))\right)$ $D_n = -C_n - \cosh(mx_1)$
Region III	$A^{III} = \mu_0 \sum_{n=1}^{\infty} \frac{J_n}{m^2} E_n \left(e^{m(x-h)} - e^{-m(x-h)}\right) \sin(my)$	$E_n = C_n e^{mh} + \frac{1}{2} e^{m(h-x_2)}$

For a coil with a constant current density j, we have

$$J_n = \frac{2j}{n\pi} \left[\cos\left(\frac{n\pi y_1}{H}\right) - \cos\left(\frac{n\pi y_2}{H}\right) \right]. \qquad (17)$$

Substituting the Fourier series (16) into (7) and dropping the z subscript, we have

$$\frac{\partial^2 A}{\partial x^2} + \frac{\partial^2 A}{\partial y^2} = -\mu_0 \sum_{n=1}^{\infty} J_n \sin\left(\frac{n\pi y}{H}\right). \qquad (18)$$

If we consider a solution as

$$A = \sum_{n=0}^{\infty} X_n(x) \sin(my) \quad , \quad m = \frac{n\pi}{H}. \qquad (19)$$

Then, flux parallel boundary conditions at y = 0, L is satisfied. Substituting (19) into (18), we obtain

$$\sum_{n=0}^{\infty} \frac{\partial^2 X_n}{\partial x^2} \sin(my) - m^2 \sum_{n=1}^{\infty} X_n \sin(my) =$$
$$-\mu_0 \sum_{n=1}^{\infty} J_n \sin(my). \qquad (20)$$

Since the sine functions are orthogonal, we can equate corresponding coefficients on both sides of this equation. We obtain

$$\frac{\partial^2 X_n}{\partial x^2} - m^2 X_n = -\mu_0 J_n. \qquad (21)$$

The solution to (21) consists of a homogeneous solution and a particular solution

$$X_n = C_n e^{mx} + D_n e^{-mx} + \frac{\mu_0 J_n}{m^2}. \qquad (22)$$

Thus, the solution (19) is given explicitly as

$$A = \sum_{n=1}^{\infty} = \left(C_n e^{mx} + D_n e^{-mx} + \frac{\mu_0 J_n}{m^2}\right) \sin(my) \qquad (23)$$

where C_n, D_n are unknown constants that are determined by using boundary conditions. For regions I and III, the term $\mu_0 J_n / m^2$ is eliminated from (23) because the current density is zero inside these regions. Also, from the flux parallel boundary condition (A = 0) at x = 0 and x = h, it can be concluded that $D_n = -C_n$ for the solutions of the regions I and III.

Using the appropriate region label, A inside each region becomes

$$A^I = \sum_{n=1}^{\infty} C_n^I (e^{mx} - e^{-mx}) \sin(my) \qquad (24)$$

$$A^{II} = \sum_{n=1}^{\infty} \left(C_n^{II} e^{mx} + D_n^{II} e^{-mx} + \frac{\mu_0 J_n}{m^2}\right) \sin(my) \quad (25)$$

$$A^{III} = \sum_{n=1}^{\infty} D_n^{III} \left(e^{m(x-h)} - e^{-m(x-h)}\right) \sin(my). \quad (26)$$

All solutions already satisfy the boundary conditions at y = 0, L. The unknown constants must be determined by satisfying the boundary conditions at x = x_1, x_2. The vector potential must be continuous across the interfaces. Otherwise, the magnetic field density B will contain infinities. Thus, at x = x_1, (24) and (25) must be equal to each other. Since this must be satisfied for all y, we obtain

$$C_n^I \left(e^{mx_1} - e^{-mx_1}\right) = C_n^{II} e^{mx_1} + D_n^{II} e^{-mx_1} + \frac{\mu_0 J_n}{m^2}. \quad (27)$$

Similarly at x = x_2, using (25) and (26), we obtain

$$C_n^{II} e^{mx_2} + D_n^{II} e^{-mx_2} + \frac{\mu_0 J_n}{m^2} = D_n^{III} \left(e^{m(x_2-h)} - e^{-m(x_2-h)}\right). \quad (28)$$

In addition to the continuity of A at the interfaces between regions, according to Maxwell's equations, the tangential component of H should be continuous across these interfaces. Since B is proportional to H in all regions, the tangential B components must be continuous. Thus, we require that $\partial A/\partial x$ be continuous at x = x_1, x_2.

At x = x_1, we obtain

$$C_n^I \left(e^{mx_1} + e^{-mx_1}\right) = C_n^{II} e^{mx_1} - D_n^{II} e^{-mx_1}. \qquad (29)$$

Similarly, at x = x_2

$$C_n^{II} e^{mx_2} - D_n^{II} e^{-mx_2} = D_n^{III} \left(e^{m(x_2-h)} + e^{-m(x_2-h)}\right). \qquad (30)$$

Equations (27)–(30) are solved simultaneously in order to find the unknown constants. The final solutions with their corresponding constants are summarized in Table II.

B. Inductance Calculation

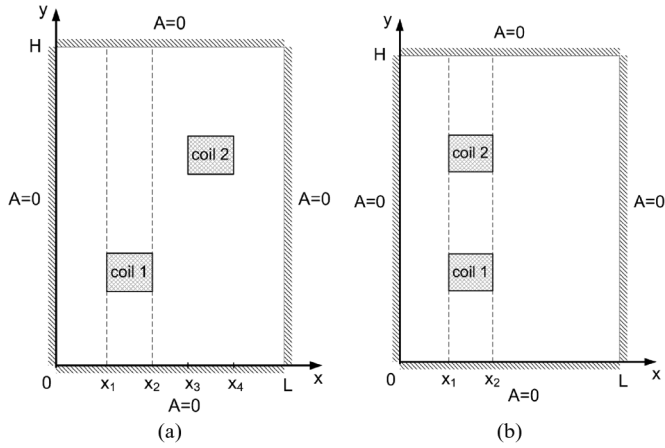In Fig. 7(a), two coils inside the core window are shown which are in different radial positions. We need the region I

Fig. 7. Calculation of mutual inductance of two coils in (a) different radial positions and (b) the same radial positions.

Fig. 8. Geometrical configuration of the transformer [17].

solution for coil 2. By substituting for A and J in (4), after some algebraic manipulation, we obtain

$$M_{12,\text{different radial positions}} = \frac{\mu_0 H}{2 I_1 I_2} \sum_{n=1}^{\infty} \frac{J_{n,1} J_{n,2}}{m^3} B_{n,2}$$
$$\times \left((e^{mx_2} - e^{mx_1}) + (e^{-mx_2} - e^{-mx_1}) \right) \quad (H) \quad (31)$$

where $M_{12,\text{ different radial positions}}$ is the mutual inductance (per unit length) of two coils in different radial positions.

If the coils are two coils axially displaced (i.e., two coils occupy the same radial position) [see Fig. 7(b)], then A_2 is the solution of region II. Thus, we have

$$M_{12,\text{ same radial positions}} = \frac{\mu_0 H}{2 I_1 I_2}$$
$$\sum_{n=1}^{\infty} \frac{J_{n,1} J_{n,2}}{m^3} \left(C_{n,1}(e^{mx_2} - e^{mx_1}) - D_{n,1}(e^{-mx_2} - e^{-mx_1}) \right.$$
$$\left. + m(x_2 - x_1) \right) \quad (H) \quad (32)$$

where $M_{12,\text{ same radial positions}}$ is the mutual inductance (per unit length) of two axially displaced coils. It is important to note that for the calculation of $B_{n,2}$, x_3 and x_4 must be substituted for x_1 and x_2 in the formulas given in Table II.

V. CONSIDERATION FOR SKIN EFFECT REDUCTION OF THE SELF INDUCTANCES

For a conductor, in addition to the "external inductance" involving a magnetic field outside the conductor (due to the total current in the conductor), there is also a much smaller component of "internal inductance" due to the magnetic field inside the conductor itself. At very high frequencies, due to the skin effect, the currents are concentrated near the surface of the conductor and since there is essentially no current deeper in the conductor, there is no magnetic field beneath the surface of the conductor. So the internal inductance of a conductor vanishes at very high frequencies.

Therefore, for the correction of the self inductance of a conductor at very high frequencies, we can simply subtract the internal inductance of the conductor from its total inductance. For conductors with a small square cross section, the internal inductance of round conductors that is equal to $\mu_0/(8\pi)$ can be used
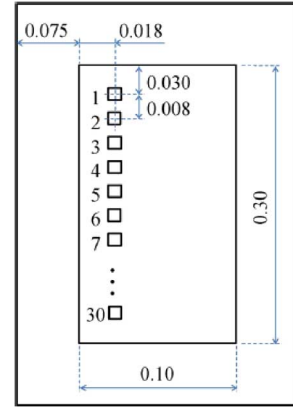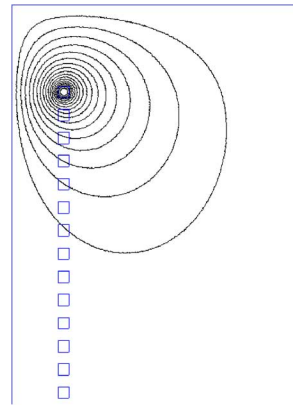

Fig. 9. Flux distribution obtained by FEM analysis.

for this purpose. As a result, in order to account for the impact of the skin effect on the self inductances at very high frequencies, the value of $\mu_0/(8\pi)$ should be subtracted from the calculated inductance values.

The proximity effect between conductors with a small cross section is negligible and, therefore, the proposed formulas can be used directly for calculation of the mutual inductances of conductors with enough accuracy.

VI. TEST CASE

The transformer winding used in [17] is applied to test the methods proposed in this paper (Fig. 8). It consists of 30 turns with a square cross-sectional area of 4×4 mm. The distance between centers of contiguous turns is 8 mm. The core window dimensions are $W = 0.1$ m, $H = 0.3$ m.

FEM simulations were performed using the free available software FEMM [23]. The core internal walls are replaced by magnetic insulation boundaries. Fig. 9 shows a flux distribution obtained by FEM analysis inside the core window. The self and mutual inductances are calculated by applying the flux linkage method.

Tables III and IV show representative values for the self and mutual inductances outside the core window, respectively. They have been computed with the method described in Section II and then compared with FEM simulations. Relative differences between results are also given and compared with the method of

TABLE III
PERCENT DIFFERENCE IN THE SELF INDUCTANCE OUTSIDE THE CORE WINDOW

Self L [μH] (per unit length)		Percent Difference [%]	
Proposed Method	FEM	Proposed Method	Method of Images [17] (average)
0.60046	0.59989	0.1	0.22

TABLE IV
PERCENT DIFFERENCE IN THE MUTUAL INDUCTANCE OUTSIDE THE CORE WINDOW

	Mutual L [μH] (per unit length)		Percent Difference [%]	
	Proposed Method	FEM	Proposed Method	Method of Images [17]
$L_{1,2}$	0.30553	0.30539	0.05	1.12
$L_{1,3}$	0.18021	0.18009	0.06	0.83
$L_{1,4}$	0.11784	0.11775	0.10	0.86
$L_{1,5}$	0.08178	0.08166	0.15	0.95
$L_{1,6}$	0.05933	0.05921	0.21	1.05
$L_{1,7}$	0.04463	0.04450	0.29	1.17
$L_{1,9}$	0.02749	0.02736	0.48	1.40
$L_{1,12}$	0.01547	0.01534	0.85	1.78
$L_{1,15}$	0.00983	0.00970	1.35	2.21
$L_{1,17}$	0.00761	0.00748	1.74	2.52
$L_{1,21}$	0.00494	0.00481	2.70	3.23
$L_{1,30}$	0.00238	0.00225	5.67	5.67

TABLE V
PERCENT DIFFERENCE IN THE SELF INDUCTANCE INSIDE THE CORE WINDOW

	Self L [μH] (per unit length)		Percent Difference [%]	
	Proposed Methods	FEM	Proposed Methods	Method of Images [17]
$L_{1,1}$	0.56793	0.56774	0.03	0.37
$L_{2,2}$	0.57760	0.57741	0.03	0.13
$L_{3,3}$	0.58273	0.58254	0.03	0.00
$L_{4,4}$	0.58559	0.58539	0.03	0.13
$L_{5,5}$	0.58723	0.58704	0.03	0.17
$L_{6,6}$	0.58820	0.58800	0.03	0.26
$L_{7,7}$	0.58877	0.58858	0.03	0.34
$L_{9,9}$	0.58932	0.58913	0.03	0.39
$L_{12,12}$	0.58957	0.58937	0.03	0.54
$L_{15,15}$	0.58962	0.58942	0.03	0.60
$L_{17,17}$	0.58962	0.58942	0.03	0.61
$L_{21,21}$	0.58952	0.58933	0.03	0.52
$L_{30,30}$	0.57760	0.57741	0.03	0.18

TABLE VI
PERCENT DIFFERENCE IN THE MUTUAL INDUCTANCE INSIDE THE CORE WINDOW

	Mutual L [μH] (per unit length)		Percent Difference [%]	
	Proposed Methods	FEM	Proposed Methods	Method of Images [17]
$L_{1,2}$	0.27873	0.27872	0.04	0.85
$L_{1,3}$	0.15753	0.15754	0.00	0.59
$L_{1,4}$	0.09831	0.09831	0.00	0.61
$L_{1,5}$	0.06464	0.06464	0.00	0.65
$L_{1,6}$	0.04411	0.04411	0.00	0.70
$L_{1,7}$	0.03097	0.03097	0.00	0.72
$L_{1,9}$	0.01624	0.01625	0.00	0.76
$L_{1,12}$	0.00680	0.00681	0.00	0.79
$L_{1,15}$	0.00303	0.00303	-0.01	0.79
$L_{1,17}$	0.00180	0.00180	0.01	0.79
$L_{1,21}$	0.00065	0.00065	-0.02	0.79
$L_{1,30}$	0.00006	0.00006	-0.14	0.79

distance. It is noticeable that all of the inductance values shown in Tables III–VI are calculated with constant current densities inside conductors.

One can also observe that the differences outside the core window are somewhat larger than the differences inside the core window. This is basically due to the errors of FEM simulations introduced in the open boundary problems.

Typically, the FEM is best suited for problems with closed solution regions. For open boundary problems, the simplest way to proceed is to pick an arbitrary boundary far enough away from the area of interest and declare A = 0 on this boundary. The truncation of the outer boundary causes error in the solution. It was observed that by increasing the volume of the outer region and using a relatively fine mesh, the results of the FEM simulation approach the results of the proposed method, and the relative differences become smaller than the values shown in Tables III and IV.

VII. CONCLUSION

New analytical methods have been established for computing the winding inductance matrix at very high frequencies. For the region outside the core window, a simple method has been developed wherein only two well-behaved integrals need to be evaluated numerically in order to determine the inductances. For the region inside the core window, accurate formulas for the self and mutual inductances have been derived from the direct solution of Poisson's equation in two different approaches. The final expressions are simple and fast convergent. The accuracy of the proposed formulas has been verified by comparisons with finite-element analyses.

APPENDIX
GAUSS-LEGENDRE QUADRATURE OVER A QUADRILATERAL ELEMENT

Consider the double integral

$$I = \int_{-1}^{1} \int_{-1}^{1} f(\xi, \eta) d\xi d\eta \tag{33}$$

images [17]. Although only a few digits are shown in the results, the relative differences are computed using full precision.

Tables V and VI show selected values for the self and mutual inductances inside the core window, respectively. Since (15) and (32) produce the same results up to 6 digits, the results of them are shown in the same column. The results are also compared with FEM simulations and the corresponding relative differences are included.

It can be noticed from Tables III–VI that the self and mutual inductances are in very close agreement to FEM simulations and nearly in all cases, the differences are considerably smaller than the image method's. It can be seen that the calculation error of mutual inductances increases with the separation
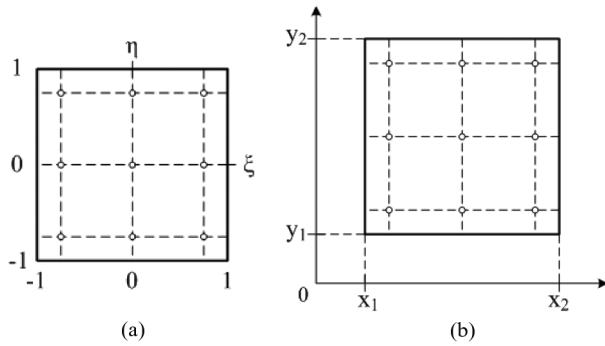
Fig. 10. Mapping an arbitrary rectangle into the standard rectangle. (a) Standard rectangle. (b) Arbitrary rectangle.

TABLE VII
WEIGHTS AND COORDINATES OF THE INTEGRATION POINTS [24]

$\pm \xi_i$	A_i	$\pm \xi_i$	A_i
n=2		*n=5*	
0.577 350	1.000 000	0.000 000	0.568 889
n=3		0.538 469	0.478 629
0.000 000	0.888 889	0.906180	0.236 927
0.774 597	0.555 556	*n=6*	
n=4		0.238 619	0.467 914
0.339 981	0.652 145	0.661 209	0.360 762
0.861 136	0.347 855	0.932 470	0.171 324

over the rectangular element shown in Fig. 10(a). Evaluating each integral, in turn, by the Gauss–Legendre quadrature using n nodes in each coordinate direction, we obtain

$$I = \sum_{i=1}^{n} \sum_{j=1}^{n} A_i A_j f(\xi_i, \eta_j). \tag{34}$$

The number of integration points n in each coordinate direction is called the integration order. The weights and the coordinates of the integration points are as listed in Table VII.

In order to apply quadrature to an arbitrary rectangle element in Fig. 10(b), it is required first to map the element into the "standard" rectangle in Fig. 10(a). The transformation that does the job is

$$x(\xi) = \frac{x_1 + x_2}{2} + \frac{x_2 - x_1}{2}\xi \quad y(\eta) = \frac{y_1 + y_2}{2} + \frac{y_2 - y_1}{2}\eta \tag{35}$$

where x_1, x_2, y_1, and y_2 are shown in Fig. 10(b).

It can be shown that the following formula for the Gauss–Legendre quadrature over an arbitrary rectangle area is obtained

$$I = \left(\frac{x_2 - x_1}{2}\right)\left(\frac{y_2 - y_1}{2}\right) \sum_{i=1}^{n} \sum_{j=1}^{n} A_i A_j f\left[x(\xi_i), y(\eta_j)\right]. \tag{36}$$

The ξ and η coordinates of the integration points and the weights can again be obtained from Table VII.

REFERENCES

[1] L. Rabins, "A new approach to the analysis of impulse voltages and gradients in transformer windings," *AIEE Trans.*, vol. 78, no. 4, pp. 1784–1791, Feb. 1960.

[2] P. I. Fergestad and T. Henriksen, "Transient oscillations in multi-winding transformers," *IEEE Trans. Power App. Syst.*, vol. PAS-93, no. 2, pp. 500–509, Mar./Apr. 1974.

[3] W. J. Mc Nutt, T. J. Blalock, and R. A. Hinton, "Response of transformer windings to system transient voltages," *IEEE Trans. Power App. Syst.*, vol. PAS-93, no. 2, pp. 457–466, Mar./Apr. 1974.

[4] A. Miki, T. Hosoya, and K. Okuyama, "A calculation method for impulse voltage distribution and transferred voltage in transformer windings," *IEEE Trans. Power App. Syst.*, vol. PAS-97, no. 3, pp. 930–939, May/Jun. 1978.

[5] F. De León and A. Semlyen, "Reduced order model for transformer transients," *IEEE Trans. Power Del.*, vol. 7, no. 1, pp. 361–369, Jan. 1992.

[6] F. De León and A. Semlyen, "Efficient calculation of elementary parameters of transformers," *IEEE Trans. Power Del.*, vol. 7, no. 1, pp. 376–383, Jan. 1992.

[7] F. De León and A. Semlyen, "Time domain modeling of eddy current effects for transformer transients," *IEEE Trans. Power Del.*, vol. 8, no. 1, pp. 271–279, Jan. 1993.

[8] E. E. Mombello, "Impedances for the calculation of electromagnetic transients within transformers," *IEEE Trans. Power Del.*, vol. 17, no. 2, pp. 479–488, Apr. 2002.

[9] K. J. Cornick, B. Filliat, C. Kieny, and W. Muller, "Distribution of very fast transient overvoltages in transformer windings," CIGRE Rep., 1992, pp. 12–204.

[10] Y. Shibuya, S. Fujita, and N. Hosokawa, "Analysis of very fast transient overvoltage in transformer winding," *Proc. Inst. Elect. Eng., Gen. Transm. Distrib.*, vol. 144, no. 5, Sep. 1997.

[11] Y. Shibuya, S. Fujita, and E. Tamaki, "Analysis of very fast transients in transformer," *Proc. Inst. Elect. Eng., Gen. Transm. Distrib.*, vol. 148, no. 5, pp. 377–383, 2001.

[12] M. Popov, L. V. Sluis, G. C. Paap, and H. de Herdt, "Computation of very fast transient overvoltages in transformer windings," *IEEE Trans. Power Del.*, vol. 18, no. 4, pp. 1268–1274, Oct. 2003.

[13] E. Bjerkan and H. K. Høidalen, "High frequency fem-based power transformer modeling: Investigation of internal computation of very fast transient overvoltages in transformer windings stresses due to network initiated overvoltages," presented at the Int. Conf. Power Syst. Transients, Montreal, QC, Canada, Jun. 19–23, 2005.

[14] G. Liang, H. Sun, X. Zhang, and X. Cui, "Modeling of transformer windings under very fast transient overvoltages," *IEEE Trans. Electromagn. Compat.*, vol. 48, no. 4, pp. 621–627, Nov. 2006.

[15] M. Popov, L. van der Sluis, R. P. P. Smeets, and J. Lopez Roldan, "Analysis of very fast transients in layer-type transformer windings," *IEEE Trans. Power Del.*, vol. 22, no. 1, pp. 238–247, Jan. 2007.

[16] S. M. H. Hosseini, M. Vakilian, and G. B. Gharehpetian, "Comparison of transformer detailed models for fast and very fast transient studies," *IEEE Trans. Power Del.*, vol. 23, no. 2, pp. 733–741, Apr. 2008.

[17] P. Gomez and F. de Leon, "Accurate and efficient computation of the inductance matrix of transformer windings for the simulation of very fast transients," *IEEE Trans. Power Del.*, vol. 26, no. 3, pp. 1423–1431, Jul. 2011.

[18] Z. Azzouz, A. Foggia, L. Pierrat, and G. Meunier, "3D finite element computation of the high frequency parameters of power transformer windings," *IEEE Trans. Magn.*, vol. 29, no. 2, pp. 1407–1410, Mar. 1993.

[19] D. J. Wilcox, M. Conlon, and W. G. Hurley, "Calculation of self and mutual impedances for coils on ferromagnetic cores," *Proc. Inst. Elect. Eng.*, vol. 135, no. 7, pp. 470–476, Sep. 1988, h A.

[20] A. Boyajian, "Leakage reactance of irregular distributions of transformer windings by the method of double fourier series," *AIEE Trans. Power App. Syst.*, vol. 29, no. 2, pt. 3, pp. 1078–1086, Jan. 1954.

[21] L. Rabins, "Transformer reactance calculations with digital computers," *AIEE Trans.*, vol. 75, pt. I, pp. 261–267, 1956.

[22] R. M. Del Vecchio, B. Poulin, P. T. Feghali, D. M. Shah, and R. Ahuja, "Transformer design principles with applications to core-form power transformers," in , 2nd ed.   Boca Raton, FL: CRC, 2010.

[23] D. C. Meeker, Finite Element Method Magnetics. ver. 4.0.2. [Online]. Available: http://www.femm.foster-miller.net, (03.12.2006 Build)

[24] J. Kiusalaas, *Numerical Methods in Engineering with MATLAB.* Cambridge, U.K.: Cambridge Univ. Press, 2005.

M. Eslamian, photograph and biography not available at the time of publication.

B. Vahidi (SM'04), photograph and biography not available at the time of publication.